

Electron-phonon coupling and electron self-energy in electron-doped graphene: calculation of angular resolved photoemission spectra.

Matteo Calandra¹ and Francesco Mauri¹

¹*CNRS and Institut de Minéralogie et de Physique des Milieux condensés,
case 115, 4 place Jussieu, 75252, Paris cedex 05, France*

(Dated: May 30, 2018)

We obtain analytical expressions for the electron self-energy and the electron-phonon coupling in electron-doped graphene using electron-phonon matrix elements extracted from density functional theory simulations. From the electron self-energies we calculate angle resolved photoemission spectra. We demonstrate that the measured kink at ≈ -0.2 eV from the Fermi level is actually composed of two features, one at ≈ -0.195 eV due to the twofold degenerate E_{2g} mode, and a second one at ≈ -0.16 eV due to the A_1' mode. The electron-phonon coupling extracted from the kink observed in ARPES experiments is roughly a factor of 5.5 larger than the calculated one. This disagreement can only be partially reconciled by the inclusion of resolution effects. Indeed we show that a finite resolution increases the apparent electron-phonon coupling by underestimating the renormalization of the electron velocity at energies larger than the kinks positions. The discrepancy between theory and experiments is thus reduced to a factor of ≈ 2.2 . From the linewidth of the calculated ARPES spectra we obtain the electron relaxation time. A comparison with available experimental data in graphene shows that the electron relaxation time detected in ARPES is almost two orders of magnitudes smaller than what measured by other experimental techniques.

PACS numbers: 74.70.Ad, 74.25.Kc, 74.25.Jb, 71.15.Mb

Despite the fact that the band structure of graphene is calculated in many solid-state textbooks [1, 2], its experimental verification has been provided only recently by Angular Resolved Photo-Emission (ARPES) measurements on a graphene monolayer deposited on a SiC substrate [3, 4, 5, 6]. The experiments show that the peculiar features of the electronic structure predicted theoretically are qualitatively confirmed by experiments: the carbon π -bands (i) cross at the K-point in the Brillouin-zone (Dirac point) and (ii) depart linearly with a slope v_f from the Dirac point, (iii) the Fermi velocity extracted from experiments [3, 5] is slightly larger (10-20%) than that calculated theoretically using density functional theory (DFT).

Beside this encouraging agreement between theory and experience, recent angular photoemission (ARPES) experiments [6, 7] performed on graphene revealed remarkable surprises. Two kinks are seen in the ARPES dispersion: the first one is at energies of 0.2 eV below the Fermi level (ϵ_f) and its energy position respect to ϵ_f is unchanged as a function of the doping level while the second one is closer to the Dirac point and its energy position respect to ϵ_f decreases rapidly as the doping level is increased (see Fig. 2 in Ref. [6]). The first kink has been attributed to a phonon feature [6], while the second kink has been interpreted as due to a plasmon [6, 8]. In what follows we focus on the first kink.

The ARPES momentum distribution curves (MDCs) associated to the -0.2 eV kink display a puzzling behavior as a function of doping. Indeed it is observed that the magnitude of the jump associated to the MDC-linewidth in the $-0.5 \text{ eV} < \epsilon - \epsilon_f < 0 \text{ eV}$ energy window decreases as a function of doping (see Fig. 3 in Ref. [6], where from top to bottom the jump increases). This is surpris-

ing since if this jump is associated to the electron-phonon interaction then it should reflect the imaginary part of the electron self-energy due to the electron-phonon interaction. Since the magnitude of such interaction is usually proportional to the density of states at the Fermi level, the jump should increase as the doping level is increased. Thus the opposite behavior should be expected. This contradiction can be solved by noting that at low doping the tail of the second peak (attributed to a plasmon), is fairly close in energy and could affect the low energy part of the momentum distribution curve. At larger dopings [9] the plasmon peak has no effect, the electron phonon coupling does increase as a function of doping. Thus we focus in the doping region identified by $\epsilon_f > 0.3$ eV (the energy-zero being at the Dirac point).

In this work we calculate the electron-phonon coupling parameter and the electron-phonon coupling contribution to the electron self-energy in doped graphene. In particular, we give an explicit demonstration of eq. 1 in ref. [10]. From the electron self-energy we obtain the spectral-weight function and the ARPES spectra. Finally we compare the calculated spectra with available experimental data, discussing in the details the important finite-resolution effects.

The paper is structured as follows. In section I) we obtain an analytical expression for the electron-phonon coupling in doped graphene. The electron self-energy is calculated in sec. II. The ARPES spectra are calculated from the electron self-energy in sec. III, including finite resolution effects. Finally in sec. IV we compare the electron relaxation time measured by different experimental techniques for both electron-doped graphene and graphite. Sec. V is devoted to conclusions.

I. ELECTRON-PHONON COUPLING IN DOPED GRAPHENE

In units of $2\pi/a$ with $a = 2.46\text{\AA}$, the 2D volume of the graphene Brillouin-zone (BZ) is $\Omega = \frac{2}{\sqrt{3}}$. The graphene π^* bands are linear with slope $\beta = \hbar v_f = 5.52\text{eV\AA}$ (within DFT) close to the Dirac points $\mathbf{K} = (1/3, 1/3, 0)$ and $\mathbf{K}' = 2\mathbf{K}$. The density of states per spin at a general energy ϵ above or below the Dirac point, but still in the region where the π^* bands can be considered linear, can thus be written as

$$N_\sigma(\epsilon) = \frac{2\pi\sqrt{3}|\epsilon|}{\beta^2} = \frac{4\pi|\epsilon|}{\Omega\beta^2}. \quad (1)$$

Note that in this work energies are always measured respect to the Dirac point.

The electron-phonon coupling for a mode ν at momentum \mathbf{q} due to the π^* bands in graphene is given by:

$$\lambda_{\mathbf{q}\nu} = \frac{2}{\hbar\omega_{\mathbf{q}\nu}N_\sigma(\epsilon_f)} \int_{BZ} \frac{d\mathbf{k}}{\Omega} |g_{\mathbf{k}\pi^*\mathbf{k}+\mathbf{q}\pi^*}|^2 \times \delta(\epsilon_{\mathbf{k}} - \epsilon_f)\delta(\epsilon_{\mathbf{k}+\mathbf{q}} - \epsilon_f) \quad (2)$$

where $\omega_{\mathbf{q}\nu}$ is the phonon frequency of the mode ν at momentum \mathbf{q} and $g_{\mathbf{k}\pi^*\mathbf{k}+\mathbf{q}\pi^*}$ is the electron-phonon matrix element for the π^* -band $\epsilon_{\mathbf{k}}$ and for the phonon mode ν .

To illustrate how the integral is evaluated we introduce the following two regions of space, namely the sets:

$$\mathcal{F}_{\mathbf{K}}(\epsilon) = \{\mathbf{k} | \beta|\mathbf{k} - \mathbf{K}| < \epsilon + \eta\} \quad (3)$$

$$\mathcal{F}_{\mathbf{K}'}(\epsilon) = \{\mathbf{k} | \beta|\mathbf{k} - \mathbf{K}'| < \epsilon + \eta\} \quad (4)$$

In these definitions, η is a small positive quantity. For $\epsilon = \epsilon_f$, since we assume that the Fermi level is not too far from the Dirac point so that the π^* bands are linear, $|\mathbf{k} - \mathbf{K}|$ or $|\mathbf{k} - \mathbf{K}'|$ is a small but finite vector and $\mathcal{F}_{\mathbf{K}}(\epsilon_f) \cap \mathcal{F}_{\mathbf{K}'}(\epsilon_f)$ is empty. The boundary of each region of space at $\eta = 0$ (circumference) is indicated as $\partial\mathcal{F}_{\mathbf{K}}(\epsilon_f)$ and $\partial\mathcal{F}_{\mathbf{K}'}(\epsilon_f)$.

In Eq. 2, the two δ -functions restrict the \mathbf{k} integrations to the region of space satisfying the conditions $\epsilon_{\mathbf{k}} = \epsilon_f$ and $\epsilon_{\mathbf{k}+\mathbf{q}} = \epsilon_f$. The set of \mathbf{k} points such that $\epsilon_{\mathbf{k}} = \epsilon_f$ is composed by the set $\partial\mathcal{F}_{\mathbf{K}}(\epsilon_f) \cup \partial\mathcal{F}_{\mathbf{K}'}(\epsilon_f)$. Thus in the integral in Eq. 2, two cases are given (labeling $\mathbf{k}' = \mathbf{k} + \mathbf{q}$):

$$(i) \mathbf{k}, \mathbf{k}' \in \partial\mathcal{F}_{\mathbf{K}}(\epsilon_f) \text{ or } \mathbf{k}, \mathbf{k}' \in \partial\mathcal{F}_{\mathbf{K}'}(\epsilon_f),$$

$$(ii) \mathbf{k} \in \partial\mathcal{F}_{\mathbf{K}}(\epsilon_f), \mathbf{k}' \in \partial\mathcal{F}_{\mathbf{K}'}(\epsilon_f) \text{ or vice versa}$$

In case (i) scattering occurs at $\mathbf{q} = \mathbf{\Gamma} + \tilde{\mathbf{q}}$, with small $\tilde{\mathbf{q}}$, and π^* bands can only couple to the twofold degenerate E_{2g} phonon mode. In case (ii) scattering occurs at $\mathbf{q} = \mathbf{K} + \tilde{\mathbf{k}}$ or at $\mathbf{q} = \mathbf{K}' + \tilde{\mathbf{k}}$, with small $\tilde{\mathbf{k}}$, and π^* bands can only couple to the A_1' phonon mode [11]. The electron-phonon matrix elements involved in the two scattering

process have been fitted to *ab initio* data in Ref. [11] and are:

$$|g_{\mathbf{K}+\tilde{\mathbf{k}}\pi^*, \mathbf{K}+\tilde{\mathbf{k}}+\tilde{\mathbf{q}}\pi^*}^{E_{2g}}|^2 = \langle g_{\mathbf{\Gamma}}^2 \rangle [1 \pm \cos(\theta_{\tilde{\mathbf{k}}, \tilde{\mathbf{q}}} + \theta_{\tilde{\mathbf{k}}, \tilde{\mathbf{k}}+\tilde{\mathbf{q}}})] \quad (5)$$

$$|g_{\mathbf{K}+\tilde{\mathbf{k}}\pi^*, \mathbf{K}'+\tilde{\mathbf{k}}+\tilde{\mathbf{q}}\pi^*}^{A_1'}|^2 = \langle g_{\mathbf{K}}^2 \rangle [1 + \cos(\theta_{\tilde{\mathbf{k}}, \tilde{\mathbf{k}}+\tilde{\mathbf{q}}})] \quad (6)$$

In Eq. 5 the \pm sign refers to the LO/TO E_{2g} modes respectively, $\langle g_{\mathbf{\Gamma}}^2 \rangle = 0.0405\text{eV}^2$ and $\langle g_{\mathbf{K}}^2 \rangle = 0.0994\text{eV}^2$, and $\theta_{\mathbf{u}, \mathbf{v}}$ is the minimal angle between the two vectors \mathbf{u}, \mathbf{v} .

For case (i) one has

$$\begin{aligned} \lambda_{\tilde{\mathbf{q}}E_{2g}} &= \frac{2 \times 2 \times 2 \langle g_{\mathbf{\Gamma}}^2 \rangle_F}{\hbar\omega_{\tilde{\mathbf{q}}E_{2g}}N_\sigma(\epsilon_f)} \int_{\mathcal{F}_{\mathbf{\Gamma}}(\epsilon_f)} \frac{d^2\tilde{\mathbf{k}}}{\Omega} \times \\ &\quad \times \delta(\epsilon_{\mathbf{K}+\tilde{\mathbf{k}}} - \epsilon_f)\delta(\epsilon_{\mathbf{K}+\tilde{\mathbf{k}}+\tilde{\mathbf{q}}} - \epsilon_f) = \\ &= \frac{8 \langle g_{\mathbf{\Gamma}}^2 \rangle_F}{\hbar\omega_{\tilde{\mathbf{q}}E_{2g}}N_\sigma(\epsilon_f)} I_{\tilde{\mathbf{q}}} \end{aligned} \quad (7)$$

where

$$\mathcal{F}_{\mathbf{\Gamma}}(\epsilon) = \{\mathbf{k} | \beta k < \epsilon + \eta\}. \quad (8)$$

The 8 prefactor is the results of having 2 E_{2g} modes and of having an identical integral over the second Fermi surface sheet at \mathbf{K}' . The integral $I_{\tilde{\mathbf{q}}}$ is the so-called nesting factor, defined as:

$$I_{\tilde{\mathbf{q}}} = \int_{\mathcal{F}_{\mathbf{\Gamma}}(\epsilon_f)} \frac{d^2\tilde{\mathbf{k}}}{\Omega} \delta(\epsilon_{\mathbf{K}+\tilde{\mathbf{k}}} - \epsilon_f)\delta(\epsilon_{\mathbf{K}+\tilde{\mathbf{k}}+\tilde{\mathbf{q}}} - \epsilon_f) \quad (9)$$

The electron-phonon coupling due to E_{2g} modes is given by

$$\lambda_{\mathbf{\Gamma}}(\epsilon_f) = N(\epsilon_f) \int_{\mathcal{F}_{\mathbf{\Gamma}}(2\epsilon_f)} \frac{d^2\tilde{\mathbf{q}}}{\Omega} \lambda_{\tilde{\mathbf{q}}E_{2g}} = \frac{2N(\epsilon_f)\langle g_{\mathbf{\Gamma}}^2 \rangle_F}{\hbar\omega_{\mathbf{\Gamma}E_{2g}}} \quad (10)$$

where we have used that

$$\int_{\mathcal{F}_{\mathbf{\Gamma}}(2\epsilon_f)} \frac{d^2\tilde{\mathbf{q}}}{\Omega} I_{\tilde{\mathbf{q}}} = N_\sigma^2(\epsilon_f)/4 \quad (11)$$

and we have replaced the E_{2g} phonon frequency with its value at $\mathbf{\Gamma}$.

Similarly, case (ii) leads to

$$\begin{aligned} \lambda_{\mathbf{K}+\tilde{\mathbf{q}}A_1'} &= \frac{2 \times 2 \langle g_{\mathbf{K}}^2 \rangle_F}{\hbar\omega_{\mathbf{K}+\tilde{\mathbf{q}}A_1'}N_\sigma(\epsilon_f)} \int_{\mathcal{F}_{\mathbf{K}}(\epsilon_f)} \frac{d^2\tilde{\mathbf{k}}}{\Omega} [1 - \cos(\theta_{\tilde{\mathbf{k}}, \tilde{\mathbf{k}}+\tilde{\mathbf{q}}})] \times \\ &\quad \times \delta(\epsilon_{\mathbf{K}'+\tilde{\mathbf{k}}} - \epsilon_f)\delta(\epsilon_{\mathbf{K}'+\tilde{\mathbf{k}}+\tilde{\mathbf{q}}} - \epsilon_f) = \\ &= \frac{4 \langle g_{\mathbf{K}}^2 \rangle_F}{\hbar\omega_{\mathbf{K}+\tilde{\mathbf{q}}A_1'}N_\sigma(\epsilon_f)} J_{\mathbf{K}+\tilde{\mathbf{q}}} \end{aligned} \quad (12)$$

and the additional factor of 2 is a result of having scattering from $\mathcal{F}_{\mathbf{K}}(\epsilon_f)$ to $\mathcal{F}_{\mathbf{K}'}(\epsilon_f)$ and vice versa. The quantity,

$$\begin{aligned} J_{\mathbf{K}+\tilde{\mathbf{q}}} &= \int_{\mathcal{F}_{\mathbf{K}}(\epsilon_f)} \frac{d^2\tilde{\mathbf{k}}}{\Omega} [1 - \cos(\theta_{\tilde{\mathbf{k}}, \tilde{\mathbf{k}}+\tilde{\mathbf{q}}})] \times \\ &\quad \times \delta(\epsilon_{\mathbf{K}'+\tilde{\mathbf{k}}} - \epsilon_f)\delta(\epsilon_{\mathbf{K}'+\tilde{\mathbf{k}}+\tilde{\mathbf{q}}} - \epsilon_f) \end{aligned} \quad (13)$$

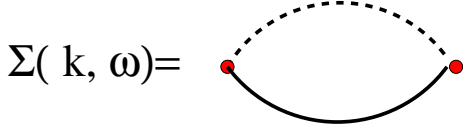


FIG. 1: Lowest order contribution to the electron self-energy due to the electron-phonon interaction. The dotted (continuous) line represents the phonon (electron) self-energy.

and its integral over the momentum $\tilde{\mathbf{q}}$ are evaluated in sec. VII A, so that the contribution of the A'_1 mode to the electron-phonon coupling is:

$$\lambda_{\mathbf{K}}(\epsilon_f) = \int_{\mathcal{F}_{\mathbf{K}(2\epsilon_f)}} \frac{d^2\tilde{\mathbf{q}}}{\Omega} \lambda_{\mathbf{K}+\tilde{\mathbf{q}}A'_1} = \frac{\langle g_{\mathbf{K}}^2 \rangle_F N_{\sigma}(\epsilon_f)}{\hbar\omega_{\mathbf{K}A'_1}} \quad (14)$$

where we have approximated $\omega_{\mathbf{K}+\tilde{\mathbf{q}}A'_1} \approx \omega_{\mathbf{K}A'_1}$.

The total electron phonon coupling is thus:

$$\lambda(\epsilon_f) = N_{\sigma}(\epsilon_f) \left[\frac{2\langle g_{\Gamma}^2 \rangle_F}{\hbar\omega_{\Gamma E_{2g}}} + \frac{\langle g_{\mathbf{K}}^2 \rangle_F}{\hbar\omega_{\tilde{\mathbf{q}}A'_1}} \right] \quad (15)$$

which is eq. 1 in ref. [10]

II. ELECTRON SELF-ENERGY AND ANGLE RESOLVED PHOTOEMISSION

The lowest contribution to the retarded electron self-energy due to coupling of π^* electrons to a phonon mode ν is illustrated in Fig. 1. At zero temperature direct calculation [12] of the diagram gives:

$$\Sigma_{\nu}(\mathbf{k}, \epsilon) = \sum_{\alpha=\{-1,1\}} \int_{BZ} \frac{d^2\mathbf{q}}{\Omega} |g_{\mathbf{k}\pi^*,\mathbf{k}+\mathbf{q}\pi^*}^{\nu}|^2 \times \left[\frac{\Theta(\alpha\epsilon_f - \alpha\epsilon_{\mathbf{k}+\mathbf{q}})}{\epsilon + i\delta - (\epsilon_{\mathbf{k}+\mathbf{q}}) + \alpha\hbar\omega_{\mathbf{q}\nu}} \right] \quad (16)$$

where $\Theta(x)$ is the Heaviside function. The imaginary part of eq. 16 is

$$\begin{aligned} \Sigma_{\nu}''(\mathbf{k}, \epsilon) &= -\pi \sum_{\alpha=\{-1,1\}} \int_{BZ} \frac{d^2\mathbf{q}}{\Omega} |g_{\mathbf{k}\pi^*,\mathbf{k}+\mathbf{q}\pi^*}^{\nu}|^2 \\ &\times \Theta(\alpha\epsilon_f - \alpha\epsilon_{\mathbf{k}+\mathbf{q}}) \delta(\epsilon - \epsilon_{\mathbf{k}+\mathbf{q}} + \alpha\hbar\omega_{\mathbf{q}\nu}) = \\ &= -\pi \sum_{\alpha=\{-1,1\}} \Theta(\alpha\epsilon_f - \alpha\epsilon - \hbar\omega_{\mathbf{q}\nu}) \\ &\times \int_{BZ} \frac{d^2\mathbf{k}'}{\Omega} |g_{\mathbf{k}\pi^*,\mathbf{k}'\pi^*}^{\nu}|^2 \delta(\epsilon - \epsilon_{\mathbf{k}'} + \alpha\hbar\omega_{\mathbf{k}'-\mathbf{k}\nu}) \quad (17) \end{aligned}$$

In angular resolved photoemission (ARPES) experiments the graphene is electron-doped, so the Fermi level is larger than the Dirac point but it is still in the region where $\epsilon_{\mathbf{k}}$ can be considered linear. For a given mode ν and a given value of α , the δ -function in eq. 17 restricts

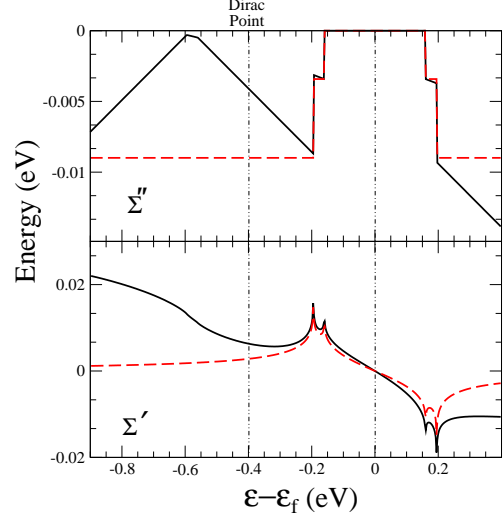


FIG. 2: (Color online) Real (Σ') and imaginary (Σ'') parts of the electron self-energy in graphene (continuous line). Dashed lines refer to self-energy parts obtained using a constant density of states. The Fermi level is $\epsilon_f = 0.4$ eV

the BZ integration to two regions, close to \mathbf{K} and to \mathbf{K}' . The restriction to these regions of k-space and the fact that we are interested in the region of energy-momentum close to the Dirac point, namely $\mathbf{k} = \mathbf{K} + \tilde{\mathbf{k}}$ with $\tilde{\mathbf{k}}$ small, restricts furthermore the integration region. Indeed it implies that for small $\tilde{\mathbf{q}}$: (i) $\mathbf{q} = \tilde{\mathbf{q}}$ and (ii) $\mathbf{q} = \mathbf{K} + \tilde{\mathbf{q}}$. Case (i) represents scattering to phonons close to the Γ point while (ii) to phonons close to the \mathbf{K} point. So the situation is similar to the previous electron-phonon calculation.

The total self-energy, $\Sigma'' = \sum_{\nu=\{E_{2g}, A'_1\}} \Sigma''_{\nu}$, due to the two E_{2g} phonon modes at Γ and to the A'_1 phonon mode at \mathbf{K} is obtained substituting Eqs. 5 and 6 in Eq. 17, assuming a constant phonon dispersion around Γ and \mathbf{K} and performing the integration over the BZ, as

$$\begin{aligned} \Sigma''(\tilde{\mathbf{k}}, \epsilon) &= -\frac{\pi}{2} \sum_{\alpha=\{-1,1\}} \left[\hbar\omega_{\Gamma E_{2g}} \lambda_{\Gamma}(\epsilon - \alpha\hbar\omega_{\Gamma E_{2g}}) \times \right. \\ &\times \Theta(\alpha\epsilon_f - \alpha\epsilon - \hbar\omega_{\Gamma E_{2g}}) + \hbar\omega_{\mathbf{K}A'_1} \lambda_{\mathbf{K}}(\epsilon - \alpha\hbar\omega_{\mathbf{K}A'_1}) \times \\ &\left. \times \Theta(\alpha\epsilon_f - \alpha\epsilon - \hbar\omega_{\mathbf{K}A'_1}) \right] \quad (18) \end{aligned}$$

where $\lambda_{\Gamma}(\epsilon - \hbar\omega_{\Gamma E_{2g}})$ and $\lambda_{\mathbf{K}}(\epsilon - \hbar\omega_{\mathbf{K}A'_1})$ are defined in Eq. 10 and in Eq. 14, respectively. From Eq. 18 we note that for small $\tilde{\mathbf{k}}$ the imaginary part of the phonon self-energy is momentum-independent, so in what follows we drop the $\tilde{\mathbf{k}}$ -label. Using numerical values of $\hbar\omega_{\Gamma E_{2g}} = 0.195\text{eV}$ and $\hbar\omega_{\mathbf{K}A'_1} = 0.16\text{eV}$, the $\Sigma''(\epsilon)$ is illustrated in Fig. 2 (black lines).

The imaginary part in eq. 18 has to be compared with the square well model which is obtained from Eq. 18

assuming a constant density of states. This is the commonly used approximation to interpret ARPES spectra [13, 14]. The square well model is illustrated in fig. 2 (red-dashed). In graphene this approximation is in principle not allowed due to the behavior of the density of states proportional to $|\epsilon|$ (see eq. 1). The difference between the two models becomes relevant for energies smaller than or closer to the Dirac point.

The real part of the electron self-energy can be obtained using the Kramers-Kronig relations, namely:

$$\Sigma'(\epsilon) = \frac{1}{\pi} \mathcal{P} \int_{-\infty}^{\infty} \frac{\Sigma''(\epsilon')}{\epsilon' - \epsilon} d\epsilon' \quad (19)$$

If the self-energy in Eq. 18 is used then $\Sigma'(\epsilon)$ diverges at large $|\epsilon|$ due to the $|\epsilon|$ dependence of the density of states. However this divergence is unphysical since in real graphene the linearity of the π^* bands and the consequent behavior of the density of states is only up to energies of ≈ 1.5 eV from the Dirac point. Thus for large $|\epsilon|$ the imaginary part of the phonon self-energy should be regularized. We adopted the following regularization:

$$\Sigma''_{\text{Reg}}(\epsilon) = \begin{cases} \Sigma''(\epsilon) & \text{if } |\epsilon| < \epsilon_M \\ \Sigma''(\epsilon_M) & \text{if } \epsilon_M < |\epsilon| \end{cases} \quad (20)$$

With this assumption, the calculation of the integral in eq. 19 leads to:

$$\begin{aligned} \Sigma'(\epsilon) = & -N_{\sigma}(\epsilon_f) \langle g_{\Gamma}^2 \rangle \left\{ (\epsilon + \hbar\omega_{\Gamma E_{2g}}) \left[-2 \log \left| \epsilon + \hbar\omega_{\Gamma E_{2g}} \right| + \right. \right. \\ & + \left. \log \left| (\epsilon_M + \epsilon)(\epsilon_f - \hbar\omega_{\Gamma E_{2g}} - \epsilon) \right| \right] + \\ & + \left. (\epsilon - \hbar\omega_{\Gamma E_{2g}}) \log \left| \frac{\epsilon_M - \epsilon}{\epsilon_f + \hbar\omega_{\Gamma E_{2g}} - \epsilon} \right| \right\} + \\ & - \frac{N_{\sigma}(\epsilon_f) \langle g_{\mathbf{K}}^2 \rangle}{2} \left\{ (\epsilon + \hbar\omega_{\mathbf{K}A_1'}) \left[-2 \log \left| \epsilon + \hbar\omega_{\mathbf{K}A_1'} \right| \right. \right. \\ & + \left. \log \left| (\epsilon_M + \epsilon)(\epsilon_f - \hbar\omega_{\mathbf{K}A_1'} - \epsilon) \right| \right] + \\ & + \left. (\epsilon - \hbar\omega_{\mathbf{K}A_1'}) \log \left| \frac{\epsilon_M - \epsilon}{\epsilon_f + \hbar\omega_{\mathbf{K}A_1'} - \epsilon} \right| \right\} + \\ & - N_{\sigma}(\epsilon_f) \left[\langle g_{\Gamma}^2 \rangle (\epsilon - \hbar\omega_{\Gamma E_{2g}}) + \frac{\langle g_{\mathbf{K}}^2 \rangle}{2} (\epsilon - \hbar\omega_{\mathbf{K}A_1'}) \right] \times \\ & \times \left[\log \left| \frac{\epsilon_M + \epsilon}{\epsilon_M - \epsilon} \right| \right] \end{aligned} \quad (21)$$

In practical calculations we choose $\epsilon_M = 1.5$ eV.

The real part of the electron self-energy is illustrated in Fig. 2 and is compared with the real part obtained from the Kramers-Kronig transformation of $\Sigma''(\omega)$ with a constant density of states.

In ARPES experiment the spectral weight is measured, namely [15]

$$A(\mathbf{k}, \epsilon) = \frac{-2[\Sigma''(\epsilon) + \eta]}{[\epsilon - \epsilon_{\mathbf{k}} - \Sigma'(\epsilon)]^2 + [\Sigma''(\epsilon) + \eta]^2} \quad (22)$$

where we allowed for a small constant imaginary part η to eliminate numerical instabilities. Typically $\eta = 10^{-4}$ eV

III. RESULTS

In this section we consider a Fermi level of $\epsilon_f = 0.4$ eV measured from the Dirac point. Neglecting resolution effects, the spectral function (Eq. 22) is shown in figure 3 (left). The scans presented are fixed photoelectron energy scans (the energy value is given on the left of Fig. 3 (left)) while the photoelectron momentum is varied (MDC scans). In the MDC scans two kinks are present (compare scans g and h for the first kink and scans e and d for the second), both in the spectral-weight maximum-position and linewidth.

The behavior of the MDC-maximum-position as a function of energy and momentum is illustrated in fig. 3 (right). The lower energy kink corresponds to the twofold degenerate E_{2g} mode, while the higher energy one corresponds to the A_1' mode.

The behavior of the MDC-linewidth, half-width half-maximum (HWMH), as a function of energy is shown in fig. 4. Notice that, in absence of resolution effects, the linewidth is equal to $-\beta\Sigma''(\epsilon)$. The behavior of the linewidth is compared with that of square well model typically used to interpret ARPES data. The differences are negligible at energies larger than -0.2 eV, but they are significant at lower energies and in particular at the Dirac point.

To test the robustness of the phonon features against experimental resolution we introduce the following convoluted spectral weight:

$$A_{\text{exp}}(\mathbf{k}, \epsilon) = f(\epsilon) \int_{-\infty}^{\infty} d\epsilon' \int d^3\mathbf{k}' A(\mathbf{k}', \epsilon') G_{\eta_{\epsilon}}(\epsilon' - \epsilon) G_{\eta_{\mathbf{k}}}(\mathbf{k}' - \mathbf{k}) \quad (23)$$

where $G_{\eta_x}(x)$ is a Gaussian having full-width η_x and centered in $x = 0$. The Fermi distribution is indicated with

$$f(\epsilon) = \frac{1}{\exp[(\epsilon - \epsilon_f)/k_B T] + 1} \quad (24)$$

This form of the experimental resolution assumes to have decoupled momentum and energy resolutions.

(21) We chose $\eta_{\epsilon} = 25$ meV and $\eta_{\mathbf{k}} = 0.1 \text{\AA}^{-1}$, as in recent ARPES experiments [6, 9]. The maximum position in $A_{\text{exp}}(\mathbf{k}, \epsilon)$ is plotted in Fig. 5.

As it can be seen the experimental resolution substantially smears out the two kinks so that a very weak kink is visible at -0.2 eV while the second one is almost invisible. The kink is substantially smaller than what detected in experiments [6]. The mass enhancement parameter is defined as [12, 13]:

$$\lambda = \left. \frac{\partial \Sigma'(\epsilon)}{\partial \epsilon} \right|_{\epsilon = \epsilon_f} \quad (25)$$

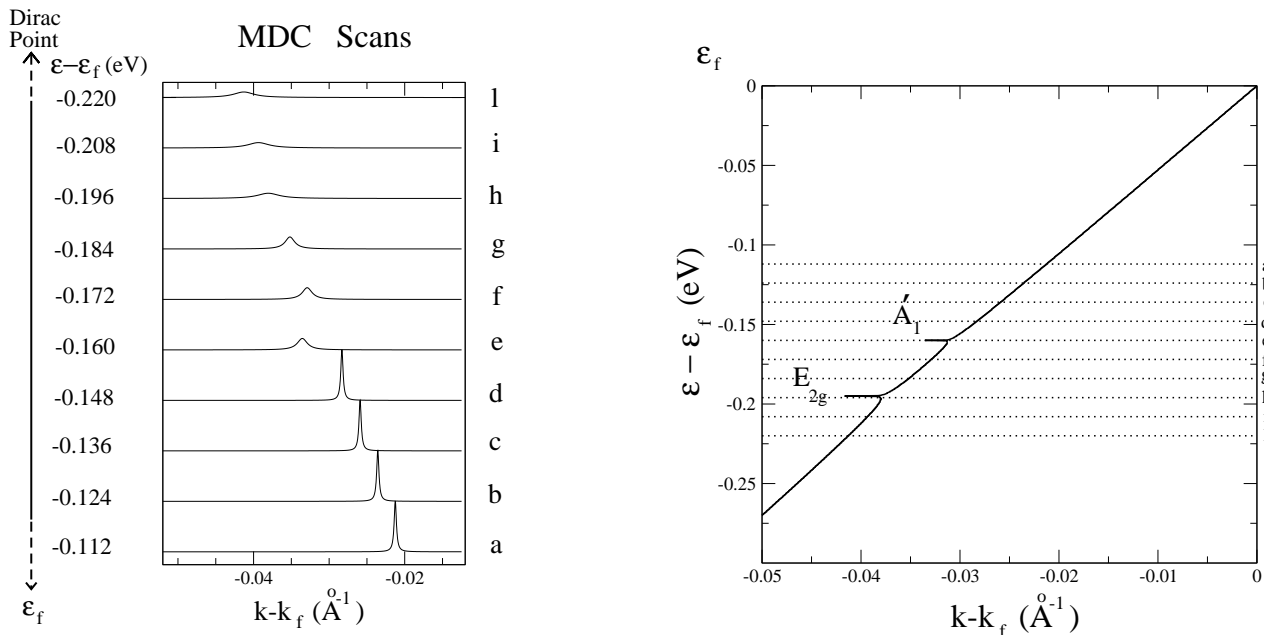


FIG. 3: MDC scans for different energies (left) and ARPES maximum position as a function of energy and momentum (right). The Fermi level is $\epsilon_f = 0.4$ eV, the experimental resolution is not included in the calculation. A 1 meV broadening is used for illustration purposes.

Linearizing $\Sigma'(\epsilon) \approx -\lambda\epsilon$, the spectral-weight becomes (for $\eta = 0$):

$$A(\mathbf{k}, \epsilon) \approx \frac{-2\Sigma''(\epsilon)Z^2}{[\epsilon - Z\epsilon_{\mathbf{k}}]^2 + [\Sigma''(\epsilon)Z]^2} \quad (26)$$

where

$$Z = \frac{1}{1 + \lambda} \quad (27)$$

is the quasiparticle weight. From Eq. 26 one sees that the quasiparticle state has quasiparticle energy $Z\epsilon_{\mathbf{k}}$ and linewidth $\Sigma''(\epsilon)Z/2$. In graphene the bands are linear, with $\epsilon_{\mathbf{k}} = \beta k$, so that the maximum position in the spectral weight at energies higher than the kink is given by the relation

$$\epsilon_{\mathbf{k}}^{\max} = \frac{\beta k}{1 + \lambda} \quad (28)$$

Assuming linear renormalized bands, $\epsilon_{\mathbf{k}} = \beta_{\text{ph}}k$, for energies larger than the kink then the following expression for λ is obtained:

$$\lambda = \frac{\beta}{\beta_{\text{ph}}} - 1 \quad (29)$$

Typically β is obtained from a linear fit to maximum position in MDC curves at energies below the kink (in our case $\beta = 5.52\text{eV}\text{\AA}$ within DFT), while β_{ph} is obtained from a linear fit at energies higher than the kink but

enough below ϵ_f so that the effects of the Fermi function in eq. 23 are absent.

When a finite resolution is used, the result is substantially affected. Indeed, we find that a linear fit in the energy window from $-0.195\text{ eV} < \epsilon - \epsilon_f < -0.04\text{ eV}$ leads to values of the electron-phonon coupling which are a factor 2.5 than Eq. 15, as shown in Fig. 6. A similar fitting procedure is used in experiments (note that in experiments only the kink due to the E_{2g} phonon is visible). A comparison with available experimental data (see fig. 5 in Ref. [9]) is shown in fig. 6. A clear disagreement between theory and experiments is still present, even if it is reduced by resolution effects.

For this reason, we believe, the determination of λ using Eq. 29 is affected by a large error. The error is due to the difficulties in the determination of β_{ph} generated by the non-linearity in $\Sigma'(\epsilon)$ near the kink. The non-linearity, when convoluted with a finite resolutions, results in a quasi-linear behavior with an “apparent” enhanced electron-phonon coupling.

IV. ELECTRON RELAXATION TIMES IN GRAPHITE AND GRAPHENE

A. Electron-doped graphene

It is interesting to compare the ARPES-measured self-energy imaginary part with what detected by alternative experimental techniques. In electron-doped graphene the

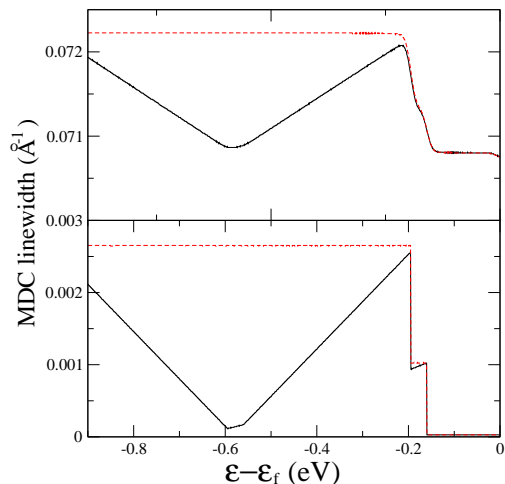


FIG. 4: (Color online) MDC - linewidth (HWHM) for the two model self-energy. The curve in upper panel is obtained using a finite resolution, while that in the lower one is without resolution effects. In the absence of resolution effects the linewidth is equal to $-\beta\Sigma''(\epsilon)$ (see fig. 1). The Fermi level is $\epsilon_f = 0.4$ eV.

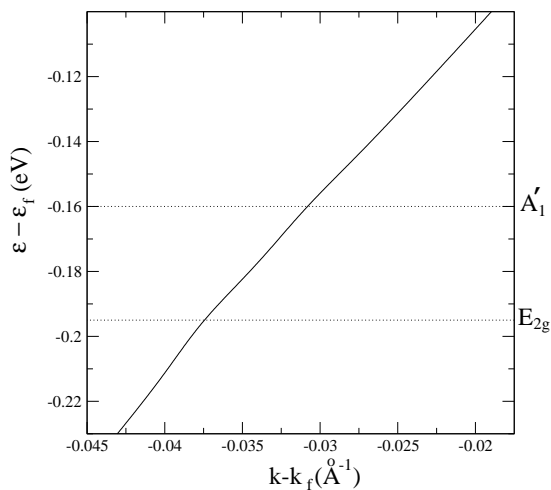


FIG. 5: Position of the maximum in MDC curves using a finite resolution. The Fermi level is $\epsilon_f = 0.4$ eV.

electron relaxation time has been determined experimentally by conductivity/mobility data [16] and by angular resolved photoemission measurements [6]. The mobility measurement detect the scattering time of electrons at energies $|\epsilon - \epsilon_f| < k_B T$, where k_B is the Boltzmann constant and T is the temperature at which the experiment

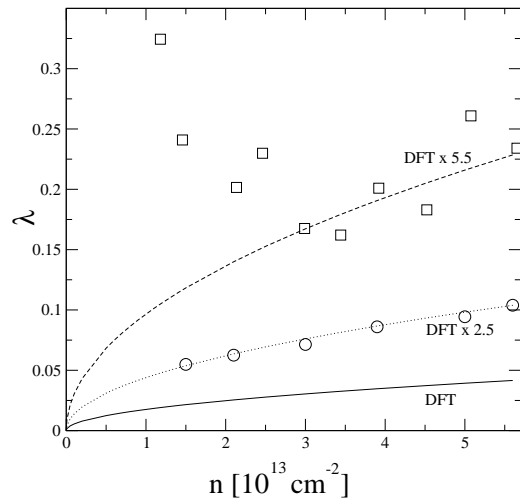


FIG. 6: Electron-phonon coupling in electron-doped graphene. The continuous line labeled DFT refers to Eq. 15, the empty squares are experimental data from Fig. 5 in ref. [9], while the empty circles represents the “apparent” electron-phonon coupling extracted from fits to the calculated ARPES spectra using Eq. 29 and including resolution effects. The curves DFT \times 5.5 and DFT \times 2.5 indicates Eq. 29 with multiplied by the prefactors 5.5 and 2.5 respectively.

is performed ($T \approx 300$ K). As shown in appendix VII B, this leads to electron scattering time of the order of

$$\tau = 0.35\text{ps} \quad (\text{from mobility}) \quad (30)$$

for $\epsilon_f > 0.2\text{eV}$. Since the Debye temperature of the optical phonon in graphene is much larger than 300 K, the scattering in the mobility measurements is mainly due to defects and acoustic phonons.

ARPES measures the electron self-energy at photo-emitted electron-energies ϵ . The imaginary part of the electron self-energy is related to the electron scattering-time by the relation $\tau(\epsilon) = \hbar/[2\Sigma''(\epsilon)]$. From the data in Refs. [6, 7] for $|\epsilon - \epsilon_f| \approx k_B T$ we obtain

$$\tau \approx 3.5\text{fs} \quad (\text{from ARPES}) \quad (31)$$

which is two order of magnitudes smaller than Eq. 30.

B. Graphite

In graphite the electron scattering time has been measured by two different experimental techniques; (i) Femtoseconds time-resolved spectroscopy [17] and (ii) ARPES.

From femtoseconds time-resolved spectroscopy [17]:

$$\begin{aligned}\tau &\approx 0.2\text{ps} \quad \text{for } |\epsilon - \epsilon_f| = 0.25 \text{ eV} \\ \tau &\approx 0.1\text{ps} \quad \text{for } |\epsilon - \epsilon_f| = 0.50 \text{ eV} \\ &\quad \text{(from femtoseconds} \\ &\quad \text{time - resolved spectroscopy)}\end{aligned}\quad (32)$$

Similar to what happens in graphene, ARPES measurements [4, 5, 18, 19] lead to a relaxation time which are two order of magnitudes times smaller than what obtained from the femtoseconds photoemission spectroscopy. For example, from the measured ARPES linewidth in Ref. [19] (see Fig. 10 c), we obtain:

$$\begin{aligned}\tau &\approx 4.7\text{fs} \quad \text{for } |\epsilon - \epsilon_f| = 0.25 \text{ eV} \\ \tau &\approx 3.4\text{fs} \quad \text{for } |\epsilon - \epsilon_f| = 0.50 \text{ eV} \\ &\quad \text{(from ARPES)}\end{aligned}\quad (33)$$

V. CONCLUSIONS

In this work we calculated the electron-phonon coupling parameter and the electron-phonon coupling contribution to the electron self-energy in doped graphene. From the electron self-energy we obtained the spectral weight function and the ARPES spectra.

The ARPES spectra as a function of momentum and energy displays two kinks. The kinks are at energies $\epsilon - \epsilon_f \approx -0.195 \text{ eV}$ and $\epsilon - \epsilon_f \approx -0.16 \text{ eV}$, where ϵ_f is the Fermi level. The two kinks are due to coupling to the twofold degenerate E_{2g} mode and to the A'_1 mode respectively. The MDC-linewidth as a function of energy is discontinuous (jump) at E_{2g} and A'_1 phonon energies.

Comparing the calculated electron-phonon coupling with that extracted from ARPES experiments we found that, for large enough electron-doping, the latter is roughly a factor 5.5 larger than the former, as suggested in ref. [9]. We partially solved this contradiction by including finite resolution effects. Indeed, in experiments the electron-phonon coupling is determined from the ratio of the electron-velocities at higher and lower energies respect to the kink. The velocities are obtained from the slopes of the maximum position of the ARPES spectra as a function of energy and momentum. We find that the slope above the kink is substantially affected by the presence of a finite resolution and the extracted values of the electron-phonon coupling are ≈ 2.5 larger than what obtained without any resolution effect. Thus when comparing calculated spectra with the inclusion of finite resolution effects to ARPES experiments [6, 9] we remark that the measured electron-phonon coupling is still a factor of 2.2 larger than the calculated one [10]. Thus this work shows once more [20] the importance of including resolution effects to correctly describe ARPES data.

Finally, from the imaginary part of the electron self-energy we obtain the electron-relaxation time. The calculated electron relaxation time is in good agreement with mobility data on electron-doped graphene

and is of the same order of magnitude of the electron relaxation time obtained from conductivity and femtoseconds time-resolved spectroscopy measurements in graphite. However this is in strong disagreement with ARPES measurements, being the ARPES relaxation times, both in graphene and graphite, almost two order of magnitudes smaller. This discrepancy essentially reflects the disagreement in the measured and calculated electron-phonon coupling. The aforementioned disagreement in the electron self-energies is even more surprising when considering that previous DFT calculations of the phonon self-energy in graphene, graphite and nanotubes were found to be in perfect agreement with experimental data for what concerns phonon dispersion and phonon lifetimes, [21, 22, 23]. Since the electron and phonon self-energies involve the same vertex, and thus the same matrix elements, a good agreement would be expected even for the electron self-energies too.

VI. ACKNOWLEDGMENTS

We acknowledge illuminating discussions with Olle Gunnarsson, Eli Rotenberg, Aaron Bostwick, Jessica McChesney and Shuyun Zhou. Calculations were performed at the IDRIS supercomputing center (project 071202).

VII. APPENDIX

A. Evaluation of the integral $J_{\mathbf{K}+\tilde{\mathbf{q}}}$

In Eq. 12, $\theta_{\tilde{\mathbf{k}}, \tilde{\mathbf{k}}+\tilde{\mathbf{q}}} = 2\theta_{\tilde{\mathbf{k}}\tilde{\mathbf{q}}} - \pi$, so that $1 - \cos(\theta_{\tilde{\mathbf{k}}, \tilde{\mathbf{k}}+\tilde{\mathbf{q}}}) = 2 \cos^2(\theta_{\tilde{\mathbf{k}}\tilde{\mathbf{q}}})$ and the integral $J_{\mathbf{K}+\tilde{\mathbf{q}}}$ (see Eq. 13) can be evaluated as:

$$\begin{aligned}J_{\mathbf{K}+\tilde{\mathbf{q}}} &= \int_0^{2\pi} d\theta_{\tilde{\mathbf{k}}\tilde{\mathbf{q}}} \int \frac{d\tilde{k}}{\Omega} 2\tilde{k} \cos^2(\theta_{\tilde{\mathbf{k}}\tilde{\mathbf{q}}}) \delta(\beta\tilde{k} - \beta k_f) \times \\ &\quad \times \delta(\beta|\tilde{\mathbf{k}} + \tilde{\mathbf{q}}| - \beta k_f) = \\ &= \frac{2\epsilon_f}{\Omega\beta^3} \int_0^{2\pi} d\theta_{\tilde{\mathbf{k}}\tilde{\mathbf{q}}} \cos^2(\theta_{\tilde{\mathbf{k}}\tilde{\mathbf{q}}}) \times \\ &\quad \times \delta(\sqrt{k_f^2 + \tilde{q}^2 + 2\tilde{k}\tilde{q} \cos(\theta_{\tilde{\mathbf{k}}\tilde{\mathbf{q}}})} - k_f) = \\ &= \frac{2k_f}{\Omega\beta^2} \sum_{\alpha=1,2} \int_{-1}^1 d(\cos(\theta_{\tilde{\mathbf{k}}\tilde{\mathbf{q}}}^\alpha)) \delta(\cos(\theta_{\tilde{\mathbf{k}}\tilde{\mathbf{q}}}^\alpha) + \frac{\tilde{q}}{2k_f}) \times \\ &\quad \times \frac{\cos^2(\theta_{\tilde{\mathbf{k}}\tilde{\mathbf{q}}}^\alpha) \sqrt{k_f^2 + \tilde{q}^2 + 2k_f\tilde{q} \cos(\theta_{\tilde{\mathbf{k}}\tilde{\mathbf{q}}}^\alpha)}}{k_f\tilde{q}|\sin(\theta_{\tilde{\mathbf{k}}\tilde{\mathbf{q}}}^\alpha)|} = \\ &= \frac{2}{\Omega\beta^2} \frac{\tilde{q}/2k_f}{\sqrt{1 - \frac{\tilde{q}^2}{4k_f^2}}}\end{aligned}\quad (34)$$

Furthermore, the integral of such a quantity is:

$$\begin{aligned}
A &= \int_{\mathcal{F}_{\mathbf{K}(2\epsilon_f)}} \frac{d^2\tilde{\mathbf{q}}}{\Omega} J_{\mathbf{K}+\tilde{\mathbf{q}}} = \\
&= \frac{2}{\Omega^2\beta^2} \int_{\mathcal{F}_{\mathbf{K}(2\epsilon_f)}} d^2\tilde{\mathbf{q}} \frac{q/2k_f}{\sqrt{1-\frac{q^2}{4k_f^2}}} = \\
&= \frac{8k_f^2}{\Omega^2\beta^2} \int_0^{2\pi} d\theta \int_0^1 dy \frac{y^2}{\sqrt{1-y^2}} = \\
&= \frac{2\pi 8k_f^2}{\Omega^2\beta^2} \left[-\frac{y\sqrt{1-y^2}}{2} + \frac{1}{2}\arcsin(y) \right]_0^1 = \\
&= \frac{16\pi k_f^2}{\Omega^2\beta^2} \frac{\pi}{4} = \frac{16\pi^2\epsilon_f^2}{\Omega^2\beta^4} \frac{1}{4} = \frac{N_{\sigma}^2(\epsilon_f)}{4} \quad (35)
\end{aligned}$$

B. From mobility to electron relaxation time

The conductivity tensor is [24]

$$\sigma = 2e^2 \sum_{\nu} \int \frac{d^2k}{(2\pi)^2} \tau_{\nu}(\mathbf{k}) \mathbf{v}_{\nu}(\mathbf{k}) \cdot \mathbf{v}_{\nu}(\mathbf{k}) \left(-\frac{\partial f}{\partial \epsilon} \right)_{\epsilon=\epsilon_{\nu}(\mathbf{k})} \quad (36)$$

Eq. 36 should then be divided by two since we are interested in only one component of the conductivity tensor. Moreover we only consider intraband transition since they are the only relevant at low temperature. The graphite bands are linear so that $\epsilon_k = \pm\beta k = \pm\hbar v_f k$ where k measure the distance from the \mathbf{K} -point. At zero temperature only electrons on the Fermi surface contribute to the inte-

gral thus, assuming a constant relaxation time, one gets:

$$\begin{aligned}
\sigma &\approx e^2 \sum_{\nu} v_f^2 \tau \int_{\mathcal{F}_{\mathbf{K}}} \frac{dkk}{(2\pi)^2} \int_0^{2\pi} d\theta \delta(\epsilon_f - \epsilon_{\mathbf{k}\nu}) = \\
&= e^2 \sum_{\nu} \frac{v_f^2 \tau}{\hbar^2 v_f^2} \frac{\epsilon_f}{\pi} = \\
&= \frac{e^2 \tau \epsilon_f}{\hbar^2 \pi} \quad (37)
\end{aligned}$$

so that

$$\tau = \frac{\hbar^2 \pi \sigma}{e^2 \epsilon_f} \quad (38)$$

The conductivity can be written as a function of the mobility as $\sigma = \delta e \mu$, where δ is the number of electrons participating in conduction per surface area. Using Eq. 1 in Ref. [22] $\delta = \epsilon_f^2/(\pi\beta^2)$ and $\sigma = \epsilon_f^2 e \mu/(\pi\beta^2)$. Thus the relaxation time becomes:

$$\tau = \frac{\hbar^2 \pi \delta \mu}{e \epsilon_f} = \frac{\hbar^2 \epsilon_f \mu}{e \beta^2} \quad (39)$$

where ϵ_f is expressed in eV and μ in $\text{cm}^2/(\text{Volt} \times \text{sec})$. Expressing the mobility in $\text{m}^2/(\text{Volt} \times \text{sec})$ one gets

$$\tau = 1.47 \times 10^{-12} \epsilon_f \mu = 1.47 \times \epsilon_f \mu \text{ ps} \quad (40)$$

Using the values of Ref. [16] for mobility one gets at large doping ($\epsilon_f > .18$ eV) values of the order of 0.35ps.

-
- [1] W. A. Harrison, *Electronic structure and the properties of solids*, Dover Publications, INC., New York, 1989, Exercise 3-3, page 95
- [2] P. R. Wallace, Phys. Rev. **71**, 622 (1947)
- [3] K. S. Novoselov, A.K. Geim, S.V. Morozov, D. Jiang, M.I. Katsnelson, I.V. Gregorieva, S. V. Dubonos, and A.A. Firsov, Nature **438**, 197 (2005)
- [4] S. Y. Zhou, G.-H. Gweon, C. D. Spataru, J. Graf, D.-H. Lee, Steven G. Louie, A. Lanzara, Phys. Rev. B **71**, 161403(R) (2005)
- [5] S. Y. Zhou, G.-H. Gweon, J. Graf, A. V. Fedorov, C. D. Spataru, R. D. Diehl, Y. Kopelevich, D.-H. Lee, Steven G. Louie, A. Lanzara, Nature Physics **2**, 595 - 599
- [6] A. Bostwick, T. Ohta, T. Seyller, K. Horn and E. Rotenberg Nature Physics **3**, 36 (2007)
- [7] S. Y. Zhou, private communication.
- [8] E. H. Hwang, B. Y. K. Hu, and S. Das Sarma, cond-mat/0612345
- [9] A. Bostwick, T. Ohta, J. L. McChesney, T. Seyller, K. Horn and E. Rotenberg, unpublished and J. McChesney, A. Bostwick, T. Ohta, T. Seyller, K. Horn, E. Rotenberg Abstract: L28.00010, APS March Meeting 2007 : *Anisotropic electron-phonon coupling in doped graphene*.
- [10] M. Calandra and F. Mauri, Phys. Rev. Lett. **95**, 237002 (2005). Note that in eq. 1 of such article there is an error in the prefactor of eq. 1. The correct prefactor is reported in Eq. 15 of the present work.
- [11] S. Piscanec, M. Lazzeri, F. Mauri, A.C. Ferrari and J. Robertson, Phys. Rev. Lett **93**, 185503 (2004)
- [12] *Many particle physics*, Gerald Mahan (third edition), Kluwer Academic/Plenum publishers, page 136
- [13] G. Grimvall, *The electron-phonon interaction in metals*, (North Holland, Amsterdam, 1981) p. 201.
- [14] T. Cuk, D. H. Lu, X. J. Zhou, Z. X. Shen, T. P. Devereaux and N. Nagaosa, Phys. Stat. Sol. (b), **242**,11 (2005)
- [15] With this definition the spectral-weight sum-rule takes the form $\int_{-\infty}^{+\infty} \frac{d\omega}{2\pi} A(\mathbf{k}, \omega) = 1$.
- [16] Y. Zhang, Y.W. Tan, H. L. Stormer, and P. Kim, Nature **438**, 201 (2005)
- [17] C. Moos, C. Gahl, R. Fasel, M. Wolf, T. Hertel, Phys. Rev. Lett. **87**, 267402 (2001)
- [18] K. Sugawara, T. Sato, S. Souma, T. Takahashi, and H. Suematsu, Phys. Rev. Lett. **98**, 036801 (2007)
- [19] S.Y. Zhou, G.-H. Gweon, A. Lanzara, Annals of Physics **321**, 1730 (2006)
- [20] See X. J. Zhou, J. Shi, T. Yoshida, T. Cuk, W. L. Yang, V. Brouet, J. Nakamura, N. Mannella, S. Komiya, Y. Ando, F. Zhou, W. X. Ti, J. W. Xiong, Z. X. Zhao, T.

- Sasagawa, T. Kakeshita, H. Eisaki, S. Uchida, A. Fujimori, Z. Zhang, E. W. Plummer, R. B. Laughlin, Z. Hussain, and Z.-X. Shen, Phys. Rev. Lett. **95**, 117001 (2005) and Phys. Rev. Lett. **96**, 119702 (2006); T. Valla, Phys. Rev. Lett. **96**, 119701 (2006)
- [21] S. Pisana, *etal.*, Nature Materials Letters **6**, 198 (2007).
- [22] M. Lazzeri and F. Mauri, Phys. Rev. Lett. **97**, 266407 (2006)
- [23] M. Lazzeri, S. Piscanec, F. Mauri, A. C. Ferrari, and J. Robertson Phys. Rev. B **73**, 155426 (2006)
- [24] *Solid State Physics*, N. W. Ashcroft and N. D. Mermin, Holy, Rinehart and Winston, 1976, page 250, Eq. 13.25